**RAA 2014** Vol. **14** No. **2**, 179–192 doi: 10.1088/1674–4527/14/2/006
*http://www.raa-journal.org* *http://www.iop.org/journals/raa*

***R**esearch in*
***A**stronomy and*
***A**strophysics*

# On properties of mass transfer in an Algol-type binary system: an example of VV Vir *

Jia Zhang[1,2,3], Sheng-Bang Qian[1,2] and Lin-Qiao Jiang[1,2,3]

[1] Yunnan Observatories, Chinese Academy of Sciences, Kunming 650011, China; *zhangjia@ynao.ac.cn*
[2] Key Laboratory of the Structure and Evolution of Celestial Objects, Chinese Academy of Sciences, Kunming 650011, China
[3] University of Chinese Academy of Sciences, Beijing 100049, China

Received 2013 August 20; accepted 2013 October 12

**Abstract** Some properties of mass transfer within a semi-detached binary system are discussed based on an example of VV Vir. The observations and analysis of VV Vir show that it is a semi-detached binary system with the less massive cooler component filling its Roche lobe, which is also called an Algol-type binary system. Based on the parameters of this semi-detached binary, a theoretical study on the mass flow is carried out, including the trajectory of the mass flow, the position, radius and temperature of the impact spot caused by the mass flow, the inconsistent form of the mass flow and the possibly huge rate of energy transfer carried by the mass flow. Humps and distortions in light curves of VV Vir are deemed to be weak evidence for the theoretical results.

**Key words:** binaries: eclipsing — stars: individual (VV Vir) — techniques: photometric

## 1 THE PARAMETERS OF VV VIR

### 1.1 Introduction of VV Vir

VV Vir (= GSC 05557–01521; $\alpha(2000) = 14^{\rm h}05^{\rm m}25.242^{\rm s}$, $\delta(2000) = -10^\circ 09' 22.31''$) bears a rich and variable history of research. Koch (1974) published findings identifying it as an 'Algol-like' binary star. Brancewicz & Dworak (1980) classified it as a contact system in their binary catalog, as did Giuricin et al. (1983). Sandage (1993) studied it not as a binary system but as an RR Lyrae variable star. Shaw (1994) reported it to be a near-contact binary system. Hoffman et al. (2006, 2008) grouped it as an Algol/$\beta$ Lyrae system based on observations from the Northern Sky Variability Survey. Samec et al. (2008) published the first high precision multi-color light curves, and listed the observational data in their paper; they deduced that it is a near-contact but detached binary system.

Four sets of light curves are analyzed together in this paper. Besides observations from the All Sky Automated Survey (ASAS) (Pojmanski & Maciejewski 2004) and Samec's paper (Samec et al. 2008), new photometric and spectroscopic observations are presented in this paper. All light curves are analyzed using the Wilson-Devinney program (Wilson & Devinney 1971; Wilson 1979, 1990;

* Supported by the National Natural Science Foundation of China.

Van Hamme & Wilson 2007; Wilson 2008). Based on the light curve solutions, we wish to draw a definite conclusion on the configuration of VV Vir.

### 1.2 Observation and Data Reduction

VV Vir was observed photometrically from 2005 March 11 to May 4 with the 1 m telescope at Yunnan Astronomical Observatory. A 1 k $\times$ 1 k CCD and the approximate standard Johnson $V$ and $I$ filters were used, and the observational data were expressed on an approximate standard system (Yang & Li 1999). The images were processed with the DAOPHOT package in IRAF[1]. The aperture for photometry was set to 1.5 times the FWHM of the stars in each image. The photometric errors[2] for individual observations were 0.002–0.02 mag in the $V$ band and 0.002–0.005 mag in the $I$ band. Differential magnitudes were determined and the comparison star's coordinate is $14^{\rm h}05^{\rm m}26.34^{\rm s}$ $-10°06'12.8''(2000)$. The check star's coordinate is $14^{\rm h}05^{\rm m}29.15^{\rm s}$ $-10°07'01.0''(2000)$. The data are listed in Table 1 and shown in the upper left panel of Figure 1. The reason for the plot of observations from the check star showing much higher scatter than the observations from VV Vir is that the check star is much fainter than VV Vir, so its signal to noise ratio is much smaller, and thus its photometric errors are much larger.

VV Vir was also observed spectroscopically on 2013 April 09–22 with the Lijiang 2.4 m telescope at Yunnan Astronomical Observatory, with the $R \sim 2200$ resolution Yunnan Faint Object Spectrograph and Camera. 185 spectra were obtained with an exposure time of 300 s each. These data were processed using IRAF. The wavelength coverage was from 5000 Å to 7800 Å. The spectrophotometric standard star is HR 5501 ($14^{\rm h}45^{\rm m}30.25^{\rm s}$ $+00°43'02.7''(2000)$). Two of the spectra are shown in Figure 2 with phases 0.0 and 0.5.

Spectrophotometry work was done to generate the light curves similar to the photometric light curves within a band. The spectral flux of wavelength range 5000–5850 Å and 5650–7200 Å was integrated to obtain the analogous Johnson $V$ and $R$ band flux respectively, and then the flux values were converted to magnitudes by $\rm mag = -2.5 \log flux - 21.1$. The two spectrophotometric light curves are shown in the lower right panel of Figure 1. It can be seen that the dispersion of the points is very large, and most of the dispersion comes from the great misalignment between different observation dates. We believe that the red points (phase 0.7–0.9) and the magenta points (phase 0.75-0.85) should overlay each other, but they have a great difference in height. The same situation is shown in that the green points (phase 0.2–0.45) and the orange points (phase 0.4–0.65) do not overlap each other. The reason for the misalignment in height is speculated as follows. In the observation of the spectrophotometric standard star, the slit of the spectrograph was not exactly centered on the star every day, so the difference in standard star flux caused the problem. If there were no misalignment, it is believed that the errors in the spectrophotometric data would not be significantly different from those of photometric data.

Besides our observations, two other sets of light curves are analyzed together in this paper. One set directly came from the table in Samec's paper (Samec et al. 2008). The data were taken on 2006 May 15–28 in Johnson-Cousins $B$, $V$, $Rc$ and $Ic$ filters at Lowell Observatory and Kitt Peak, and are shown in the upper right panel of Figure 1. The other set came from ASAS (Pojmanski & Maciejewski 2004). The data were taken from 2000 December 26 to 2009 September 11 in the $V$ filter at Las Campanas Observatory. ASAS data have five different aperture magnitudes for each individual observation, and the MAG_2 aperture magnitudes were selected for their small dispersion compared to other apertures. There are a total of 576 points for ASAS data and 8 of them are excluded due to their large dispersion. The data are shown in the lower left panel of Figure 1.

[1] Image Reduction and Analysis Facility (IRAF) is a collection of software written at the National Optical Astronomy Observatory geared toward the reduction of astronomical images in pixel array form.

[2] The photometric errors are the signal to noise ratio of the stars in the images in the form of differences in magnitude, which are directly derived from IRAF.

**Table 1** Photometry Data of VV Vir

| HJD 2,450,000+ | Δmag $V$ band | HJD 2,450,000+ | Δmag $V$ band | HJD 2,450,000+ | Δmag $V$ band | HJD 2,450,000+ | Δmag $V$ band |
|---|---|---|---|---|---|---|---|
| 3441.2673 | −1.922 | 3451.1937 | −1.844 | 3472.2445 | −1.843 | 3495.1538 | −1.838 |
| 3441.2719 | −1.926 | 3451.1993 | −1.782 | 3472.2500 | −1.894 | 3495.1576 | −1.818 |
| 3441.2763 | −1.907 | 3451.2037 | −1.704 | 3472.2555 | −1.946 | 3495.1613 | −1.784 |
| 3441.2807 | −1.911 | 3451.2084 | −1.639 | 3472.2610 | −1.961 | 3495.1650 | −1.761 |
| 3441.2851 | −1.920 | 3451.2128 | −1.526 | 3472.2666 | −1.989 | 3495.1686 | −1.740 |
| 3441.2922 | −1.920 | 3451.2172 | −1.427 | 3472.2733 | −1.986 | 3495.1724 | −1.711 |
| 3441.2966 | −1.947 | 3451.2215 | −1.348 | 3472.2790 | −1.999 | 3495.1760 | −1.725 |
| 3441.3009 | −1.942 | 3451.2261 | −1.197 | 3472.2827 | −1.998 | 3495.1797 | −1.690 |
| 3441.3053 | −1.928 | 3451.2305 | −1.072 | 3472.2864 | −2.015 | 3495.1835 | −1.687 |
| 3441.3097 | −1.928 | 3451.2349 | −0.985 | 3472.2901 | −2.004 | 3495.1875 | −1.688 |
| 3441.3140 | −1.931 | 3451.2393 | −1.033 | 3472.2938 | −1.994 | 3495.1912 | −1.706 |
| 3441.3184 | −1.919 | 3451.2437 | −1.067 | 3472.2976 | −1.992 | 3495.1949 | −1.715 |
| 3441.3228 | −1.918 | 3451.2481 | −1.193 | 3472.3013 | −2.011 | 3495.1987 | −1.727 |
| 3441.3272 | −1.938 | 3451.2524 | −1.330 | 3472.3050 | −1.996 | 3495.2025 | −1.761 |
| 3441.3315 | −1.916 | 3451.2566 | −1.468 | 3472.3088 | −1.986 | 3495.2062 | −1.776 |
| 3441.3359 | −1.921 | 3451.2608 | −1.595 | 3472.3126 | −2.004 | 3495.2099 | −1.795 |
| 3441.3403 | −1.920 | 3451.2651 | −1.650 | 3472.3164 | −1.995 | 3495.2138 | −1.813 |
| 3441.3447 | −1.871 | 3451.2694 | −1.723 | 3472.3203 | −2.002 | 3495.2175 | −1.827 |
| 3441.3491 | −1.884 | 3451.2737 | −1.787 | 3472.3242 | −2.006 | 3495.2213 | −1.844 |
| 3441.3537 | −1.888 | 3451.2779 | −1.864 | 3472.3279 | −1.992 | 3495.2251 | −1.848 |
| 3441.3580 | −1.919 | 3451.2823 | −1.933 | 3472.3315 | −1.991 | 3495.2289 | −1.857 |
| 3441.3624 | −1.895 | 3451.2868 | −1.966 | 3472.3353 | −1.978 | 3495.2326 | −1.878 |
| 3441.3669 | −1.895 | 3451.2912 | −1.990 | 3472.3390 | −1.979 | 3495.2363 | −1.871 |
| 3441.3714 | −1.889 | 3451.2957 | −2.037 | 3495.1128 | −1.997 | 3495.2401 | −1.889 |
| 3441.3760 | −1.846 | 3451.3003 | −2.043 | 3495.1166 | −1.966 | 3495.2438 | −1.904 |
| 3441.3806 | −1.815 | 3472.1952 | −1.179 | 3495.1203 | −1.988 | 3495.2475 | −1.893 |
| 3441.3851 | −1.769 | 3472.2006 | −1.055 | 3495.1240 | −1.950 | 3495.2514 | −1.919 |
| 3441.3896 | −1.722 | 3472.2061 | −0.978 | 3495.1276 | −1.955 | 3495.2551 | −1.917 |
| 3441.3941 | −1.601 | 3472.2116 | −1.036 | 3495.1315 | −1.942 | 3495.2591 | −1.899 |
| 3441.3987 | −1.526 | 3472.2170 | −1.203 | 3495.1351 | −1.935 | 3495.2630 | −1.939 |
| 3441.4033 | −1.431 | 3472.2225 | −1.378 | 3495.1389 | −1.917 | 3495.2667 | −1.925 |
| 3441.4079 | −1.284 | 3472.2281 | −1.529 | 3495.1426 | −1.902 | 3495.2704 | −1.930 |
| 3441.4127 | −1.102 | 3472.2335 | −1.649 | 3495.1463 | −1.837 | 3495.2740 | −1.945 |
| 3441.4172 | −1.033 | 3472.2390 | −1.790 | 3495.1501 | −1.868 | | |

| HJD 2,450,000+ | Δmag $I$ band | HJD 2,450,000+ | Δmag $I$ band | HJD 2,450,000+ | Δmag $I$ band | HJD 2,450,000+ | Δmag $I$ band |
|---|---|---|---|---|---|---|---|
| 3441.2697 | −1.739 | 3451.1969 | −1.645 | 3472.2463 | −1.676 | 3495.1594 | −1.584 |
| 3441.2741 | −1.740 | 3451.2015 | −1.579 | 3472.2518 | −1.731 | 3495.1631 | −1.546 |
| 3441.2785 | −1.746 | 3451.2062 | −1.529 | 3472.2574 | −1.767 | 3495.1668 | −1.516 |
| 3441.2829 | −1.753 | 3451.2106 | −1.462 | 3472.2628 | −1.795 | 3495.1705 | −1.494 |
| 3441.2873 | −1.750 | 3451.2150 | −1.375 | 3472.2684 | −1.796 | 3495.1742 | −1.466 |
| 3441.2944 | −1.755 | 3451.2194 | −1.278 | 3472.2753 | −1.795 | 3495.1779 | −1.446 |
| 3441.2988 | −1.773 | 3451.2237 | −1.192 | 3472.2808 | −1.803 | 3495.1816 | −1.441 |
| 3441.3031 | −1.762 | 3451.2283 | −1.071 | 3472.2845 | −1.810 | 3495.1853 | −1.447 |
| 3441.3075 | −1.763 | 3451.2327 | −0.993 | 3472.2882 | −1.814 | 3495.1894 | −1.451 |
| 3441.3118 | −1.763 | 3451.2371 | −0.977 | 3472.2919 | −1.815 | 3495.1931 | −1.466 |
| 3441.3162 | −1.755 | 3451.2415 | −1.000 | 3472.2956 | −1.825 | 3495.1968 | −1.489 |
| 3441.3206 | −1.762 | 3451.2459 | −1.088 | 3472.2994 | −1.816 | 3495.2006 | −1.519 |
| 3441.3250 | −1.757 | 3451.2502 | −1.192 | 3472.3032 | −1.828 | 3495.2043 | −1.556 |
| 3441.3293 | −1.750 | 3451.2545 | −1.287 | 3472.3070 | −1.821 | 3495.2080 | −1.581 |
| 3441.3337 | −1.750 | 3451.2587 | −1.384 | 3472.3107 | −1.815 | 3495.2119 | −1.594 |
| 3441.3381 | −1.747 | 3451.2629 | −1.475 | 3472.3146 | −1.808 | 3495.2157 | −1.623 |
| 3441.3425 | −1.737 | 3451.2673 | −1.541 | 3472.3184 | −1.813 | 3495.2194 | −1.657 |
| 3441.3469 | −1.715 | 3451.2715 | −1.618 | 3472.3223 | −1.821 | 3495.2233 | −1.669 |
| 3441.3513 | −1.726 | 3451.2758 | −1.662 | 3472.3261 | −1.819 | 3495.2270 | −1.690 |
| 3441.3558 | −1.712 | 3451.2800 | −1.712 | 3472.3296 | −1.804 | 3495.2307 | −1.708 |
| 3441.3602 | −1.741 | 3451.2846 | −1.761 | 3472.3334 | −1.808 | 3495.2345 | −1.718 |
| 3441.3647 | −1.711 | 3451.2890 | −1.777 | 3472.3372 | −1.804 | 3495.2381 | −1.713 |
| 3441.3692 | −1.721 | 3451.2934 | −1.805 | 3495.1184 | −1.794 | 3495.2419 | −1.729 |
| 3441.3737 | −1.694 | 3451.2981 | −1.832 | 3495.1222 | −1.790 | 3495.2456 | −1.738 |
| 3441.3783 | −1.668 | 3472.1970 | −1.045 | 3495.1258 | −1.780 | 3495.2495 | −1.738 |
| 3441.3829 | −1.601 | 3472.2024 | −0.956 | 3495.1295 | −1.767 | 3495.2533 | −1.750 |
| 3441.3873 | −1.571 | 3472.2079 | −0.936 | 3495.1333 | −1.751 | 3495.2570 | −1.754 |
| 3441.3918 | −1.508 | 3472.2134 | −1.019 | 3495.1370 | −1.741 | 3495.2611 | −1.749 |
| 3441.3964 | −1.427 | 3472.2189 | −1.158 | 3495.1407 | −1.723 | 3495.2648 | −1.751 |
| 3441.4010 | −1.347 | 3472.2244 | −1.295 | 3495.1444 | −1.699 | 3495.2685 | −1.749 |
| 3441.4057 | −1.240 | 3472.2299 | −1.417 | 3495.1482 | −1.675 | 3495.2722 | −1.755 |
| 3441.4101 | −1.145 | 3472.2353 | −1.523 | 3495.1519 | −1.648 | 3495.2759 | −1.756 |
| 3441.4149 | −1.017 | 3472.2408 | −1.603 | 3495.1556 | −1.618 | | |

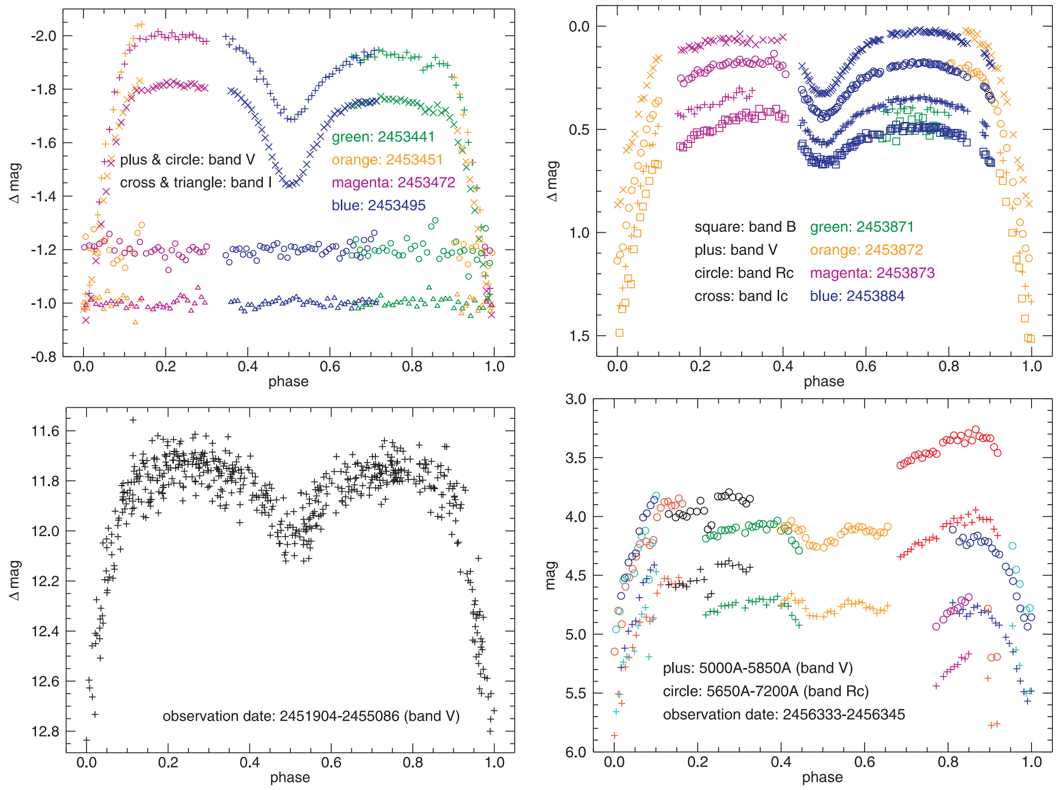


**Fig. 1** Light curves of VV Vir. *Upper left panel*: according to the photometric data. *Upper right panel*: according to Samec data (Samec et al. 2008). *Lower left panel*: according to the ASAS project (Pojmanski & Maciejewski 2004). *Lower right panel*: according to the spectrophotometric data. Different symbols represent different bands. Circles and triangles in the upper left panel stand for $\Delta$mag of the check star minus the comparison star (with a shift in mag for convenience of plotting). Different colors denote different observation dates in Heliocentric Julian Date (HJD). All the phase values are computed based on the period $P = 0.446134671$ days (Samec et al. 2008).

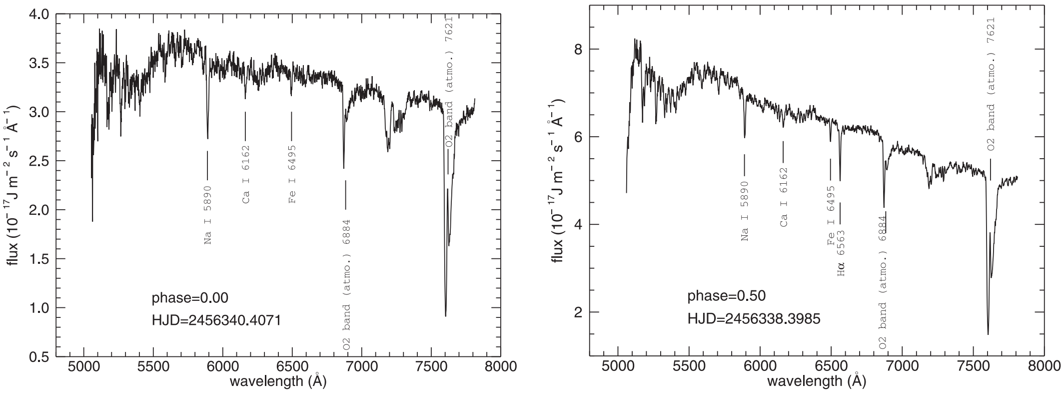


**Fig. 2** Spectra of VV Vir.

### 1.3 The Temperature of VV Vir

The temperatures of the two stars in VV Vir are derived by our spectral data. The spectra at phases 0.0 and 0.5 correspond to the secondary and primary star facing us respectively, so they are used to determine the temperature of the two stars. We compare the spectra of the phase close to 0 and 0.5 with THE 1993 KURUCZ STELLAR ATMOSPHERES ATLAS, and find that the best temperature and metallicity are $T_1 = 5750$ K and $\log{(Z_1/Z_\odot)} = 0.5$ for the primary star, and $T_2 = 4750$ K and $\log{(Z_2/Z_\odot)} = 0.5$ for the secondary star respectively. We use the IDL program Hammer[3] by Kevin R. Covey et al. to obtain the MK spectral type, which is G5–G7 for the primary star and G9–K1 for the secondary star.

There is an interesting feature in the spectra. It can be seen that the spectrum at phase 0 does not have an $\mathrm{H}\alpha$ line[4], which indicates the secondary star has no $\mathrm{H}\alpha$ line. The reason is thought to be because magnetic activity in the chromosphere generates the $\mathrm{H}\alpha$ emission line, and the emission line just fills the photospheric absorption line.

### 1.4 The Semi-detached Configuration of VV Vir

In order to deduce the configuration of VV Vir, the search for the mass ratio is done in four modes[5] using the Wilson-Devinney program, see Figure 3. In the analysis, the primary star's temperature $T_1$ is assumed to be 5750 K according to our spectral results above[6]. For the ASAS data and the spectrophotometric data, the secondary star's temperature $T_2$ is also fixed at 4750 K according to our spectral results. If $T_2$ is set to be adjustable, no convergent solution can be obtained within a reasonable range of parameters due to the large dispersion of the data.

From the photometric data in the upper left panel of Figure 3, it can be seen that mode 5 (semi-detached configuration) and mode 2 (detached configuration), shown by the thick black line, share almost the same global minimum Sum of Square Residuals (SSR). The minimum of mode 5 indicates that VV Vir is a semi-detached binary system with the less massive cooler component filling its Roche lobe. In fact, the minimum of mode 2 gives the same conclusion as mode 5 that we are going to explain. The thick black line ends at its minimum point, and there is no solution on the left side of the minimum point. At that side the Wilson-Devinney program requires the radius of the secondary star to be bigger than the radius of its Roche lobe to get a convergent solution, but this requirement contradicts the physics of a detached binary system. It can be seen that the radius of the secondary star divided by the radius of its Roche lobe in mode 2, shown by the red line, increases to one with decreasing mass ratio. When the SSR reaches the minimum, the radius of the secondary star equals the radius of its Roche lobe, which means the secondary star is in contact with its Roche lobe. The best solution of mode 2 is a semi-detached configuration which is almost the same solution as that of mode 5. The detached mode 2 once again confirms the semi-detached configuration.

From the Samec data shown in the upper right panel of Figure 3, the situation is similar. The difference is that the left end point of the thick black line is not the minimum point. Nevertheless it can be seen that at the minimum point of mode 2, the height of the red line is also close to one, more precisely, 0.99. Therefore it still indicates that the best solution is the semi-detached configuration.

---

[3] *http://www.astro.washington.edu/users/slh/hammer/*

[4] There are three observations in different dates within 9 days around phase 0, and the $\mathrm{H}\alpha$ lines are all invisible.

[5] There are different modes in the Wilson-Devinney program, and each mode corresponds to a particular geometric configuration. VV Vir is certainly within the scope of the four modes, that are: mode 2 is for detached binaries; mode 3 is for overcontact binaries; mode 4 is for semi-detached binaries with star 1 completely filling its limiting lobe (Roche lobe); mode 5 is the same as mode 4, except that it is star 2 that completely fills its limiting lobe, and this is the usual mode for Algol-type binaries.

[6] The analysis based on the primary star's temperature of 5450 K (Samec et al. 2008) is also carried out, and the solutions are almost the same as that of 5750 K for the photometric data and Samec data.

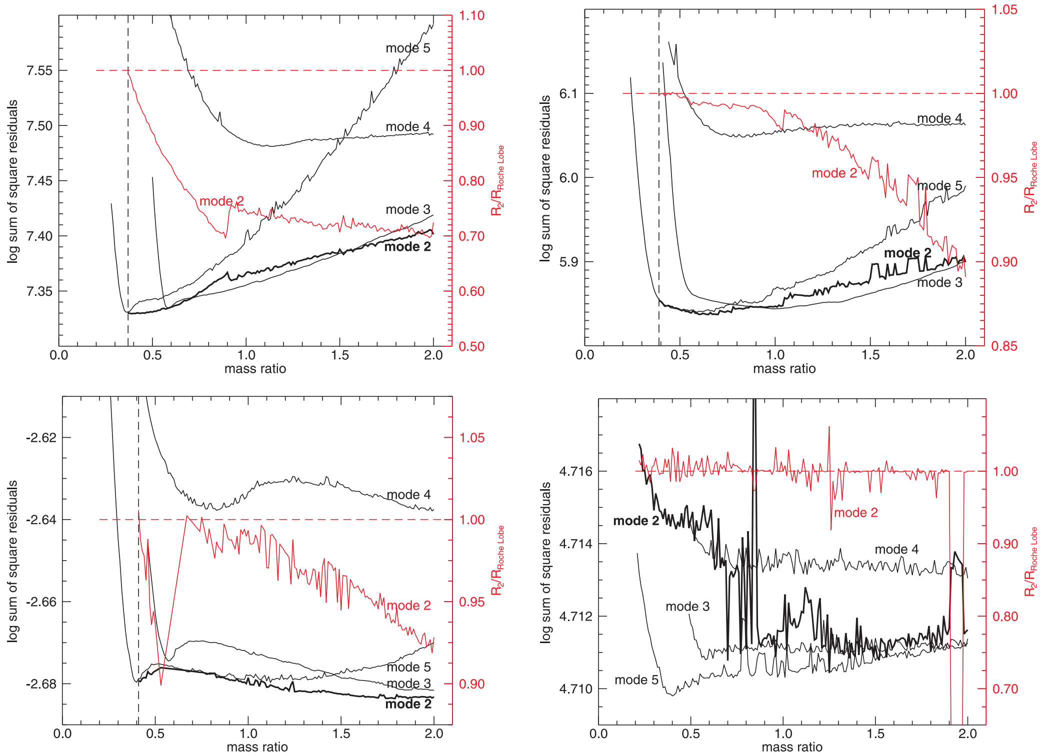


**Fig. 3** Mass ratio search diagram of VV Vir. *Upper left panel*: according to the photometric data. *Upper right panel*: according to the Samec data (Samec et al. 2008). *Lower left panel*: according to the ASAS data (Pojmanski & Maciejewski 2004). *Lower right panel*: according to the spectrophotometric data. The left ordinate is for the black lines and the right ordinate is for the red lines. The red label $R_2/R_{\rm Roche\ Lobe}$ is the radius of the secondary star divided by the radius of its Roche lobe around it in the backwards direction. Mode 2 represents detached configuration, mode 3 denotes over-contact configuration, mode 4 stands for semi-detached configuration with the hotter component filling its Roche lobe, and mode 5 represents semi-detached configuration with the cooler component filling its Roche lobe. The horizontal red dashed line indicates the height is 1 for $R_2/R_{\rm Roche\ Lobe}$. The vertical black dashed line indicates the thick black line and red line have the same end for mode 2.

From the ASAS data shown in the lower left panel of Figure 3, there is a minimum point around mass ratio 0.4 in mode 5 and mode 2 similar to the above two panels, but it is not the global minimum point. The global minimum point is in mode 2 at a mass ratio around 2. It is thought that the solution for the global minimum point should not be accepted by physics for the unreasonable case that the much more massive component has a lower temperature than its companion in a detached binary system. Therefore even though it has a better value for SSR, it is not physically possible.

From the spectrophotometric data shown in the lower right panel of Figure 3, it is obvious that mode 5 has the global minimum point. The dramatic dispersion of the red line demonstrates the large errors associated with the solutions that are caused by the great dispersion in the data.

As mentioned above, all the four sets of light curves give the same conclusion that VV Vir is a semi-detached binary system with the less massive cooler component filling its Roche lobe. The mass ratio around 0.4 is thought to be correct because it is represented in all the panels in Figure 4.

**Table 2** Solutions of VV Vir

| Parameters | Photometric data | Samec data | ASAS data | Spectrophotometric data |
|---|---|---|---|---|
| Mode | Semi-detached | Semi-detached | Semi-detached | Semi-detached |
| $i$ [°] | 89.0(±0.9) | 79.5(±0.1) | 89.0(±2.0) | 83.6(±10.8) |
| $q$ $[m_2/m_1]$ | 0.36(±0.01) | 0.59* | 0.40(±0.02) | 0.40(±0.32) |
| $T_1$ [K]* | 5750 | 5750 | 5750 | 5750 |
| $T_2$ [K] | 4668(±33) | 4322(±18) | 4750* | 4750* |
| $A_1^*$ | 0.5 | 0.5 | 0.5 | 0.5 |
| $A_2^*$ | 0.5 | 0.5 | 0.5 | 0.5 |
| $g_1^*$ | 0.32 | 0.32 | 0.32 | 0.32 |
| $g_1^*$ | 0.32 | 0.32 | 0.32 | 0.32 |
| $\Omega_1$ | 3.05(±0.02) | 3.50(±0.03) | 3.03(±0.06) | 3.09(±0.88) |
| $\Omega_2(=\Omega_{\rm in})$ | 2.60 | 3.05 | 2.68 | 2.68 |
| $L_1/(L_1+L_2)_B$ | ... | 0.908(±0.008) | ... | ... |
| $L_2/(L_1+L_2)_B$ | ... | 0.092(±0.0005) | ... | ... |
| $L_1/(L_1+L_2)_V$ | 0.844(±0.010) | 0.861(±0.008) | 0.829(±0.013) | 0.821(±0.19) |
| $L_2/(L_1+L_2)_V$ | 0.156(±0.001) | 0.139(±0.0009) | 0.171(±0.002) | 0.179(±0.03) |
| $L_1/(L_1+L_2)_{R_c}$ | ... | 0.816(±0.009) | ... | 0.790(±0.20) |
| $L_2/(L_1+L_2)_{R_c}$ | ... | 0.183(±0.001) | ... | 0.210(±0.03) |
| $L_1/(L_1+L_2)_I$ | 0.781(±0.008) | ... | ... | ... |
| $L_2/(L_1+L_2)_I$ | 0.219(±0.001) | ... | ... | ... |
| $L_1/(L_1+L_2)_{I_c}$ | ... | 0.781(±0.008) | ... | ... |
| $L_2/(L_1+L_2)_{I_c}$ | ... | 0.219(±0.001) | ... | ... |
| $r_1$ (pole) | 0.368(±0.003) | 0.340(±0.003) | 0.377(±0.01) | 0.367(±0.12) |
| $r_1$ (point) | 0.402(±0.005) | 0.375(±0.005) | 0.419(±0.02) | 0.404(±0.20) |
| $r_1$ (side) | 0.382(±0.004) | 0.351(±0.004) | 0.392(±0.01) | 0.381(±0.15) |
| $r_1$ (back) | 0.392(±0.004) | 0.364(±0.004) | 0.405(±0.01) | 0.392(±0.17) |
| $r_2$ (pole) | 0.274(±0.002) | 0.313 | 0.283(±0.004) | 0.283(±0.061) |
| $r_2$ (point) | 0.397(±0.002) | 0.446 | 0.407(±0.004) | 0.408(±0.061) |
| $r_2$ (side) | 0.286(±0.003) | 0.327 | 0.295(±0.004) | 0.295(±0.065) |
| $r_2$ (back) | 0.319(±0.003) | 0.359 | 0.327(±0.004) | 0.328(±0.064) |
| $\Sigma\text{res}^2$ | 21423965 | 692308 | 0.00209161 | 0.512607 |

∗ Assumed.

### 1.5 The Solutions of VV Vir

The final solutions are obtained based on the semi-detached mode 5, and the parameters are listed in Table 2 and shown by black lines in Figure 4. Except for the solutions of the Samec data, the other three solutions are close to each other. Amazingly, although the spectrophotometric data have very large dispersion, they can still give a consistent solution with other data. Considering the data are independent of each other, the three mutually verified solutions are thought to be correct, so the mass ratio is thought to be about 0.4.

Since almost all the primary stars in Algol systems are main sequence stars (Ibanoğlu et al. 2006), the primary star of VV Vir is assumed to be a main sequence star, which can be used to estimate its absolute parameters. According to the primary star's temperature of 5750 K, a mass of $0.95-1.02\ M_\odot$, radius of $0.88-1.30\ R_\odot$ and luminosity of $0.76-1.67\ L_\odot$ are assigned to the primary star. Then, based on the mass ratio and the relative radius from the solutions, the mass and the radius of the secondary star can be calculated, which are $0.68-1.00\ R_\odot$ and $0.38-0.41\ M_\odot$ respectively. VV Vir's parameters (orbital period, mass ratio, mass, radius and surface potential) are used as an example for discussing the properties of mass transfer (if it exists) in a semi-detached binary system.

## 2 PROPERTIES OF THE MASS FLOW

In a semi-detached binary system, there may be mass transfer from the component that fills its lobe to its companion star in the form of mass flow. In this section, the properties of the mass flow are

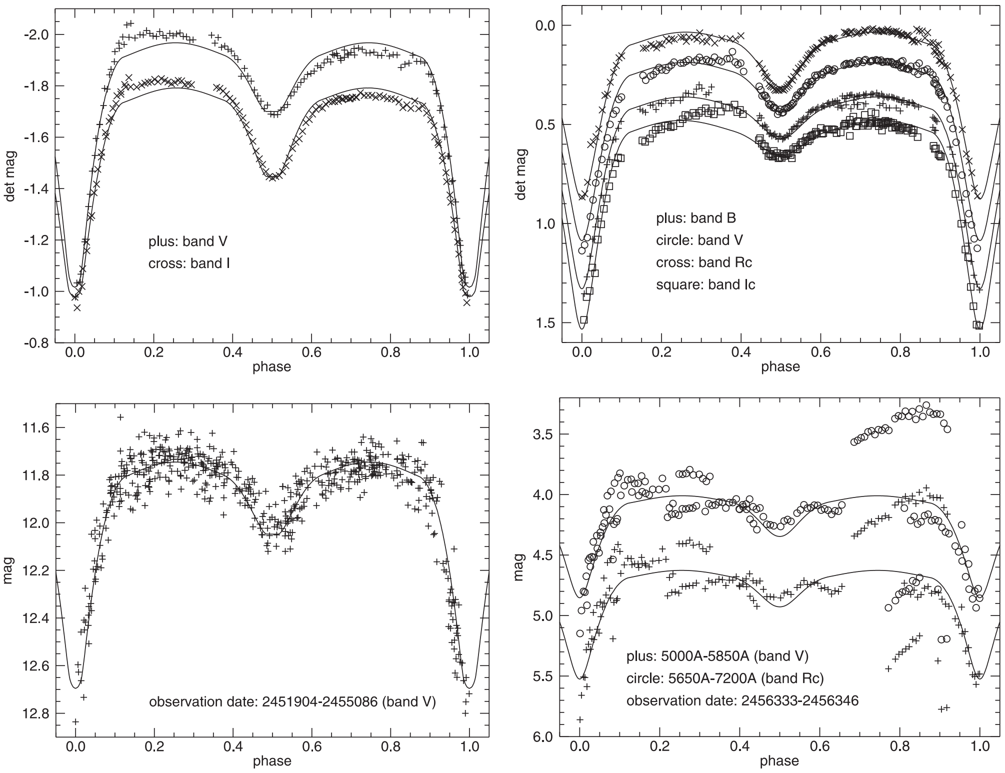


**Fig. 4** Solutions of VV Vir. *Upper left panel*: according to the photometric data. *Upper right panel*: according to the Samec data (Samec et al. 2008). *Lower left panel*: according to the ASAS data (Pojmanski & Maciejewski 2004). *Lower right panel*: according to the spectrophotometric data. Different symbols denote different bands.

studied theoretically with the parameters of VV Vir. These properties can reflect the generality of other similar systems as we will discuss later.

### 2.1 The Trajectory of the Mass Flow

Based on the mass ratio $q$ and the surface potential $\Omega$ of the two stars (see Table 2), and by the help of the subroutine ROMQ in the Wilson-Devinney program, the contours defining the boundaries of the two stars on a relative scale (the distance between the two stars is 1) are calculated and shown in Figure 5. The contours according to the photometric data, ASAS data and the spectrophotometric data are very close to each other, so we plot them together in one panel. However, the contour defined by the Samec data significantly differs from the other cases, so we plot it in another panel.

Based on the mass ratio $q$ and the orbital period of 0.446134671 days (Samec et al. 2008), the trajectory of the mass flow is calculated under the mass point model[7]. The leaf shaped curves originating from the inner Lagrange point in Figure 5 trace the trajectories. Because the trajectory is also plotted on a relative scale, it has nothing to do with the absolute masses of the stars.

[7] Two stars are seen as a mass particle without volume, and a small particle with negligible mass freely falls in the two stars' gravitational field. The small particle's falling trajectory is deemed to be the trajectory of the mass flow.

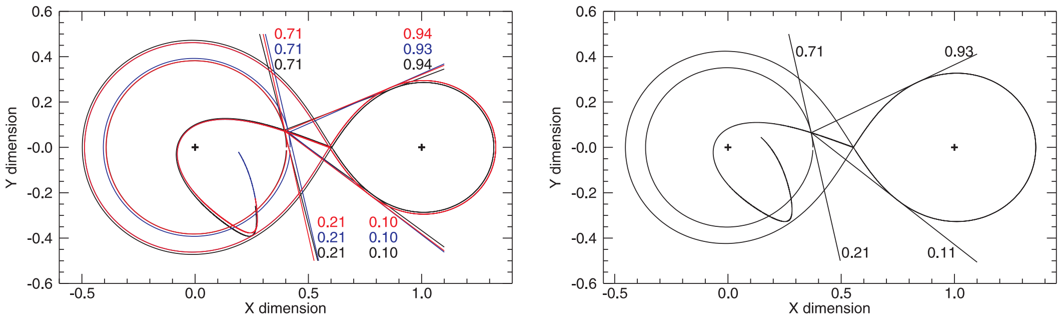


**Fig. 5** The contour and the trajectory of the mass flow for VV Vir in the plane of its orbit. *Left panel*: The black, blue and red colors correspond to photometric data, ASAS data and spectrophotometric data, respectively. *Right panel*: the contour according to the Samec data. The leaf-shaped curves originating from the inner Lagrangian point trace the calculated mass flow trajectories based on the the mass point model. The straight lines indicate the horizon of the impact spot. The numbers are the phases of the light curve corresponding to the straight lines.

### 2.2 The Radius of the Mass Flow

It is thought that the thickness of the mass flow is determined by the extent of the secondary star overfilling its Roche lobe, or say the difference between the secondary star's radius and its Roche lobe's radius. Taking into account the shape and angle of the secondary star near the inner Lagrangian point, the diameter of the outward mass flow is about 1–2 times the difference between the two radii. We cannot calculate an accurate diameter of the mass flow, but we can give an upper limit. The Tout & Eggleton (1988) mass transfer equation is used to estimate the difference in radius.

$$\dot{M} = -C\left(\ln \frac{R}{R_L}\right)^3, \tag{1}$$

where $C = 1000\ M_\odot\ \mathrm{yr}^{-1}$, $\dot{M}$ is the rate of mass transfer in $M_\odot\ \mathrm{yr}^{-1}$, $R$ is the radius of the secondary star, and $R_L$ is the radius of the Roche lobe around it (the radius of a sphere that has the same volume as the star or Roche lobe). The typical rate of mass transfer in an Algol system is $10^{-11} - 10^{-6}\ M_\odot\ \mathrm{yr}^{-1}$, which corresponds to an overfill of $0.002\% - 0.1\%$ based on Equation (1). For the case of VV Vir, the secondary star's radius is about $0.68 - 1.00\ R_\odot$, so the overfill in absolute value is about $1.5 \times 10^{-5} - 1.0 \times 10^{-3}\ R_\odot$. We speculate that the radius of the mass flow is also about this value.

The process of the mass flow falling spans a dynamical time scale. According to our calculation, it takes less than 10 hours to fall from the inner Lagrangian point to the primary star's surface. By contrast, the expansion process of a star spans a thermal or even nuclear time scale. Therefore the rapid process of falling will not allow too much mass to accumulate on the secondary star's Roche lobe. Hence, the small overfill is not surprising which leads to a thin mass flow.

### 2.3 The Rate of Energy Transfer Associated with Mass Transfer

In the process of mass transfer, the potential energy of the falling mass is converted to kinetic energy, and then is converted to heat energy. In order to model the rate of energy transfer, we first need to compute the decrement in potential energy.

The definition of $\Omega$ in the Wilson-Devinney program is (Kopal 1959)

$$\Omega := -\frac{\Psi d}{GM_1} - \frac{1}{2}\frac{q^2}{q+1}, \tag{2}$$

and

$$-\Psi = G\frac{M_1}{r_1} + G\frac{M_2}{r_2} + \frac{\omega^2}{2}r_\omega^2, \tag{3}$$

where $\Psi$ is the potential energy in joules per kilogram, $G$ the gravitational constant, $M_1$ and $M_2$ the mass of the primary and secondary star respectively, $r_1$, $r_2$ and $r_\omega$ the distance to the primary star, the secondary star, and the rotation axis, respectively, $d$ the distance between the two component stars, and $q$ and $\omega$ the mass ratio and the angular velocity of the binary system respectively. For the case of VV Vir, the change in potential energy of the mass flow from the surface of the secondary star to the surface of the primary star is given as $2.3 \times 10^{10} - 3.2 \times 10^{10}$ J kg$^{-1}$. With the typical rate of mass transfer of an Algol system $10^{-11} - 10^{-6}\ M_\odot$ yr$^{-1}$, or $6.3 \times 10^{11} - 6.3 \times 10^{16}$ kg s$^{-1}$, the rate of energy transfer is calculated as $1.4 \times 10^{22} - 2.0 \times 10^{27}$ J s$^{-1}$, or $3.8 \times 10^{-5} - 5.2\ L_\odot$.

Compared to the luminosity of the primary star $0.76 - 1.67\ L_\odot$, if the rate of mass transfer is large ($> 10^{-8}\ M_\odot$ yr$^{-1}$), the energy transfer rate is not a negligible contribution to energy for the primary star or even the main source of energy.

## 2.4 An Intermittent Form of Mass Transfer

Is the mass transfer continuous or not? In most cases it is not, as we will demonstrate. Suppose the total mass and the total angular momentum of the binary system are constant during the process of mass transfer[8], then the absolute radius of the Roche lobe for the mass donor star is only a function of the mass ratio[9], see Figure 6. It can be seen that the radius of the Roche lobe increases with decreasing mass ratio when the mass ratio is less than 0.788. (Most semi-detached binary systems have a mass ratio less than 0.788 (Ibanoğlu et al. 2006).) The mass flow leads to a decrease of mass ratio, and consequently to an increase in the Roche lobe around the mass donor star. As a result, the expanding Roche lobe will become larger than its star. When the mass donor star does not fill its Roche lobe, the mass flow must stop. The mass flow will not start again until the next time that the mass donor star expands to fill its Roche lobe. Therefore, the mass flow must be intermittent and unstable, which is similar to the case of UX Mon (Olson et al. 2009). Thus the mass flow[10] will exist sometimes but not other times, and sometimes be significant but sometimes small.

Conversely, if the mass ratio is larger than 0.788, the mass flow is continuous and sustainable (but may be not stable). The decreasing mass ratio leads to a decrease in the radius of the Roche lobe around the mass donor star. Even without the expansion of the star, mass transfer will persist until the mass ratio is less than 0.788.

## 2.5 The Impact Spot Caused by the Mass Flow

If there is mass flow in a semi-detached binary system, there should be an impact spot on the surface of the mass gainer star. The parameters of the impact spot can be calculated by the parameters of the mass flow. The position, radius and temperature of the impact spot are discussed as follows.

The intersection of the mass flow trajectory and the outline of the mass gainer star is the position of the impact spot. The mass flow should be in the orbital plane, so the latitude of the impact spot is $\pi/2$. For VV Vir, the longitude is computed as 0.191 from the photometric data, 0.158 from the ASAS data, 0.176 from the spectrophotometric data and 0.174 from the Samec data, see Figure 5.

[8] This hypothesis is not correct for systems in which magnetic braking leads to rapid loss of angular momentum.
[9] The mass ratio is defined as the ratio of the mass of the mass donor star to that of the mass gainer star.
[10] If the duration of each mass flow is very short, the mass flow may have the form of a 'mass drop.'

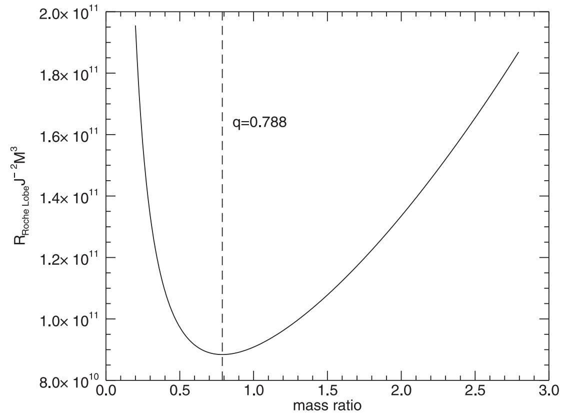


**Fig. 6** The relationship between the radius of the mass donor star's Roche lobe and the mass ratio. $R_{\rm Roche\ Lobe}$ is the radius of the mass donor star's Roche lobe, and $J$ and $M$ are the total angular momentum and total mass of the binary system respectively.

The radius of the impact spot[11] is deemed as the radius of the mass flow, which is $1.5 \times 10^{-5} - 1.0 \times 10^{-3}\ R_\odot$ for VV Vir. In the unit of radians on the surface of the mass gainer star, it is $1.1 \times 10^{-5} - 1.1 \times 10^{-3}$ radians. Even taking into account a split in the mass flow and the thermal diffusion process on the surface which will make the impact spot become bigger, it is thought that the radius of the hot impact spot is unlikely to exceed 10 times this value. A radius of 0.03 radians for the spot is shown in Figure 7 for illustration. It is believed that the real impact spot is smaller than the one in the figure, or even just a point.

The temperature of the impact spot can be calculated by the energy transfer rate of the mass transfer. From the process of impact, kinetic energy is converted to heat energy on the surface. An isobaric process with heat absorption of ideal gas is assumed here, and the heated mass will become fully ionized after the temperature rises. A simple formula is employed to calculate the increment in temperature,

$$\Delta Q = C_{\rm p} \Delta T, \tag{4}$$

where $\Delta Q$ is the heat absorption, $C_{\rm p} = \frac{5}{2}R$ the heat capacity at constant pressure with $R = 8.314\ {\rm JK^{-1}mol^{-1}}$ being the gas constant, and $\Delta T$ the temperature increment. The chemical composition of the solar surface is applied here, so a mole of completely ionized gas is 0.61 gram. The increment in temperature given by the formula is $6.8 \times 10^5 - 9.4 \times 10^5$ K, which is an extremely high temperature, and this is considered to be the temperature of the hot impact spot. Although the heat will be dissipated to the surrounding mass by diffusion and convection, the continuous energy injection (if it exists) by the mass flow will support the dissipation on a dynamical timescale. Therefore the actual temperature will be lower than the calculated value, but not by much. It is suggested that the temperature is more than 10 percent of this value.

## 3 WEAK EVIDENCE FROM VV VIR

Properties of the mass flow have been discussed above based on the parameters of VV Vir, but is there actually mass flow in VV Vir? If there is, is the mass flow in VV Vir consistent with our previous discussion? The only observational evidence we have is the distortions in the light curves which can be explained by the effect of the impact spot caused by the mass flow.

[11] It is assumed that the impact spot is round and the temperature is uniform.

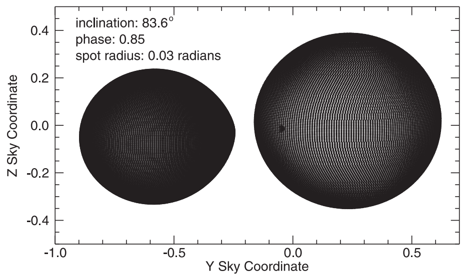


**Fig. 7** Images of VV Vir with the impact spot according to the spectrophotometric data. The dark spot identifies the impact spot.

Based on the position of the impact spot, the directions from where the spot can be seen are known. In other words, the phases of light curves affected by the spot can be modeled. The straight lines and their associated numbers in Figure 5 show that two phases are affected: 0.10–0.21 and 0.71–0.94 (0.93) for the left panel, and 0.11–0.21 and 0.71–0.93 for the right panel[12].

In the photometric observations, it is found that there are distortions in the calculated phases of the light curves, see Figure 4. The spectrophotometric light curves show, although with very large dispersions, huge humps in the calculated phases. For other light curves, if we also include the same band ($V$ and $I$) from different observations (see Fig. 8), it can be seen that both light curves show distortions at the same phase around 0.9, which is within the calculated phases.

According to our previous discussion, the radius of the impact spot is very small, and the temperature of the impact spot is extremely high. With the basic solutions of VV Vir (see Table 2), a series of light curves with very small and very hot spots are generated using the Wilson-Devinney program, see Figure 9. It can be seen that the light curves in the case of a spot can generally fit the position and shape (without the height[13]) of points around the calculated affected phases (the green points). Therefore, the humps or distortions in the affected phases are deemed to be weak but direct evidence of the existence of the mass flow with given geometric parameters.

The parameters of the impact spot are shown in the right panel of Figure 9. Radius of less than 0.02 radians and temperature larger than $5 \times 10^5$ K are beyond the computation limit of the Wilson-Devinney program, so there is no solution in that range. Different combinations of radius and temperature can give almost the same light curves, thus it can be predicted from the trend of the points that there will be solutions with combinations of higher temperature and smaller radius, and those parameters are in the range of our previous calculation.

The humps or distortions in the calculated phases of light curves vary with time, see Figure 1. This is consistent with the theoretical prediction of the intermittent behavior of the mass flow. However, the unstable humps cannot be regarded as evidence of intermittent behavior. More observations are needed to confirm this property.

Besides the humps in the calculated phases directly caused by the impact spot, the light curves also show distortions and variations in other phases (see Fig. 1). Two shoulders of the photometric light curves are unsymmetrical in height. The left shoulders of the Samec light curves exhibit a very distorted shape. Points with different colors but the same phase do not match each other, see the green points in the upper right panel of Figure 1. We speculate that the reason for the distortions and

[12] Besides the position, the inclination of the binary orbit can also affect the phases in the light curves, but the effects are small since the inclination is close to 90 degrees.

[13] In Figure 9, it can be seen that the black lines can be fit to the blue points that are not the real observational points but the translation of the green points. Why do we need this translation? The reasons are the misalignments between different observation dates that are discussed in Section 1.2.

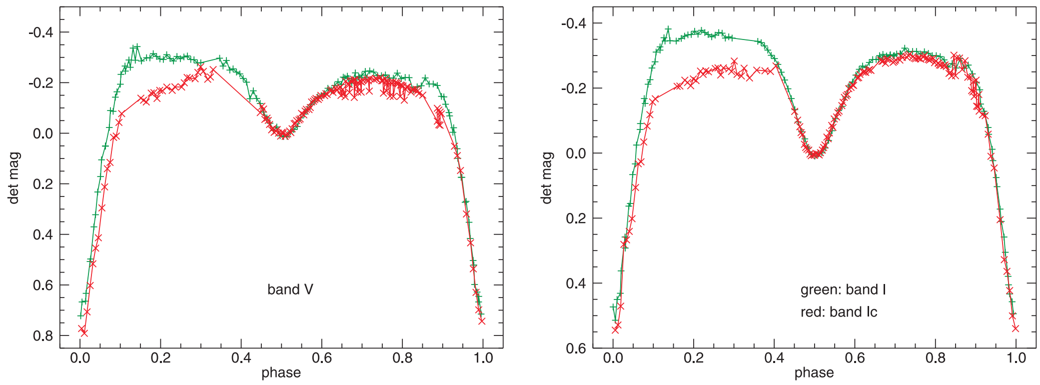


**Fig. 8** Comparison of the light curves in the same band. *Left panel*: $V$ band. *Right panel*: $I(Ic)$ band. The lines with green pluses represent the photometric data. The lines with red crosses denote the Samec data (Samec et al. 2008).

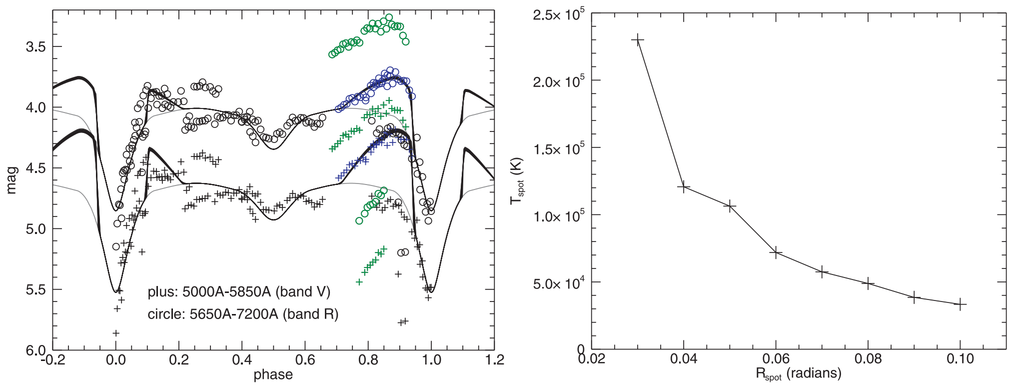


**Fig. 9** *Left panel*: The light curves in the case of a spot according to the spectrophotometric data. Different symbols represent different bands. The gray lines indicate light curves from the basic solution without a spot. The black lines denote light curves with a spot. There are eight light curves with a spot for each band overlaying each other. Each black line has a different combination of radius and temperature, but has the same position of the impact spot. The black lines exactly match the gray lines except for two affected phases. The blue points are not the real observed points but the translation of the green points. *Right panel*: The pluses stand for parameters of the impact spot of the eight light curves displayed by black lines in the left panel.

variations is also the mass flow, but indirectly. If the rate of mass transfer is large ($> 10^{-8}\ M_\odot\ \mathrm{yr}^{-1}$), the mass flow will carry a large amount of energy including gravitational and rotational energy, and transfers them from the mass donor star to mass gainer star. The large, varying amount of transferred energy leads to variations in the luminosity of the mass gainer star, thereby causing variations and distortions in the light curves, see the left shoulders in Figure 8. The envelope of the mass gainer star is convective in that its mass is less than $1.5\ M_\odot$. The convection zone can randomly transport the heat energy everywhere, so any phase in the light curve can be affected, not just the phases where the spot can be directly observed. Like the case of the unstable humps, their are not enough observations of VV Vir in this paper to support the conclusion of a large amount of energy is being transferred between the component stars, and more observations are needed.

## 4 CONCLUSIONS AND DISCUSSION

The properties of mass transfer, also called mass flow, in a semi-detached binary system are discussed in this paper, including the trajectory, radius, energy transfer rate and the form of a possible mass flow, as well as the impact spot caused by the mass flow. The parameters of the mass flow (and impact spot) are calculated based on the parameters of VV Vir. The bad observations of VV Vir are consistent with the calculated results, so VV Vir is regarded as weak evidence for the theoretical conclusions. The humps and distortions in the light curves[14] constitute evidence of mass flow, which can be directly and indirectly explained by the light effects of the hot impact spot on the surface of the star.

Although the properties of the mass flow are calculated based on a particular binary system, some of the properties can generally be used for semi-detached binary systems. First, the relative trajectory of the mass flow can be calculated with only the mass ratio and the orbital period. Second, if the rate of mass transfer is large, the energy transfer rate is comparable to, or even larger than, the intrinsic luminosity of the mass gainer star, so the stellar luminosity can be largely affected. Third, if the mass ratio is less than 0.788 (the case for most semi-detached binary systems) and the system does not have fast angular momentum loss, the mass flow (if it exists) cannot be continuous. Fourth, the mass flow will cause a very small but very hot impact spot, and the impact spot can be observed via humps in the light curves.

**Acknowledgements** This work is partly supported by the National Natural Science Foundation of China (Grant Nos. 11133007, 10973037, 10903026, 11203066 and 11003040) and by the West Light Foundation of Chinese Academy of Sciences. New photometric and spectroscopic observations of the system were obtained with the 1.0-m and 2.4-m telescopes at Yunnan Observatories.

### References

Brancewicz, H. K., & Dworak, T. Z. 1980, Acta Astronomica, 30, 501
Giuricin, G., Mardirossian, F., & Mezzetti, M. 1983, A&AS, 54, 211
Hoffman, D. I., Harrison, T. E., McNamara, B. J., et al. 2006, AJ, 132, 2260
Hoffman, D. I., Harrison, T. E., Coughlin, J. L., et al. 2008, AJ, 136, 1067
Ibanoğlu, C., Soydugan, F., Soydugan, E., & Dervişoğlu, A. 2006, MNRAS, 373, 435
Koch, R. H. 1974, AJ, 79, 34
Kopal, Z. 1959, Close Binary Systems, The International Astrophysics Series (London: Chapman & Hall)
Olson, E. C., Henry, G. W., & Etzel, P. B. 2009, AJ, 138, 1435
Pojmanski, G., & Maciejewski, G. 2004, Acta Astronomica, 54, 153
Samec, R. G., Labadorf, C. M., Behn, G. A., et al. 2008, AJ, 136, 1667
Sandage, A. 1993, AJ, 106, 703
Shaw, J. S. 1994, Mem. Soc. Astron. Italiana, 65, 95
Tout, C. A., & Eggleton, P. P. 1988, ApJ, 334, 357
Van Hamme, W., & Wilson, R. E. 2007, ApJ, 661, 1129
Wilson, R. E. 1979, ApJ, 234, 1054
Wilson, R. E. 1990, ApJ, 356, 613
Wilson, R. E. 2008, ApJ, 672, 575
Wilson, R. E., & Devinney, E. J. 1971, ApJ, 166, 605
Yang, Y., & Li, L. 1999, Publications of the Yunnan Observatory, 1, 32

[14] The spectrographic observations can also provide evidence of the mass flow, for example the emission line and the wavelength shift of lines. In fact, we did obtain the radial velocity curve of the binary system, and in the calculated affected phases the curve shows sudden changes. But the radial velocity curve is blended with two stars and we cannot deblend them, so the curve is not presented in this paper.